

Twist-2 operators induced Dark Matter Interactions

Hrishabh Bharadwaj^{a,b,#} and Sukanta Dutta^{b,\$}

^a*Department of Physics & Astrophysics, University of Delhi, Delhi, India.*

^b*SGTB Khalsa College, University of Delhi, Delhi, India.*

E-mail: # [Corresponding Author: hrishabhphysics@gmail.com](mailto:hrishabhphysics@gmail.com), \$ Sukanta.Dutta@gmail.com

ABSTRACT: We study the effective interactions of the fermionic, scalar and vector dark matter (DM) with leptons and neutral electroweak gauge Bosons induced by the higher dimensional effective twist-2 tensor operators. We constrain these lepto-philic, τ^\pm -philic and $U(1)_Y$ gauge Boson B-philic effective interactions of DM with the visible world from the WMAP and Planck data. The thermally averaged indirect DM pair annihilation cross-section and the DM-electron direct-detection cross-section for such DM candidates are observed to be consistent with the respective experimental data. Constraining coefficients of the effective operators from the low energy LEP data for the $DM \leq 80$ GeV, we further study their sensitivities in the pair production of such $DM \geq 50$ GeV in association with mono-photon at the proposed ILC and perform the χ^2 analysis to obtain the 99.73% C.L. acceptance contours in the $m_{DM} - \Lambda_{\text{eff}}$ plane from the two dimensional differential distributions of the kinematic observables. We observe that ILC has rich potential to probe the contribution of such effective operators.

KEYWORDS: Effective operators, lepto-philic, dark matter, linear collider, mono-photon.

Contents

1	Introduction	1
2	Effective interactions of lepto-philic & $U(1)_Y$ gauge Boson B-philic DM	3
3	DM Phenomenology	4
3.1	Constraints from Relic Density	4
3.2	Indirect Detection	6
3.3	DM-electron scattering	9
4	Collider sensitivity of effective operators	10
4.1	LEP Constraints on the effective operators	10
4.2	\cancel{E}_T + Mono-photon signals at ILC	11
4.3	Differential Cross-sections and χ^2 Analysis	14
5	Summary and Outlook	16
A	Thermal averaged annihilation cross-sections	18

1 Introduction

It is imperative to determine the nature of elusive *Dark Matter* (DM) [1] candidates, which constitute roughly $\sim 23\%$ of the energy density of the universe [1–6] and whose predicted relic density is ~ 0.119 [7, 8]. The most popular proposition for DM theories are weakly interacting dark matter particles (WIMPs). Features of DM interactions can be determined from the direct and indirect detection experiments apart from their direct searches in the present [9–11] and proposed colliders [12–14]. The direct detection experiments like DAMA/LIBRA [15, 16], CoGeNT [17], CRESST [18], CDMS [19], XENON100 [20, 21], LUX [22] and PandaX-II [23] are designed to measure the recoil momentum of scattered atom or nucleon by DM in the chemically inert medium of the detector, while the indirect detection experiments such as FermiLAT [24–26], HESS [27], AMS-02 [28, 29] *etc.* are looking for the evidences of the DM pair annihilation to Standard Model (SM) particles such as photons, e^+e^- , $\mu^+\mu^-$, $\tau^+\tau^-$, $\bar{b}b$ pairs and *etc.*

In last few years, many experiments like PAMELA [30, 31] have reported the excess in the positron flux (i.e., flux ratio of positron to sum of electron and positron) without any significant excess in \bar{p} channel (i.e., flux ratio of protons to anti-protons). The peaks in e^+e^- channel are also observed in ATIC [32] and PPB-BETS [33] balloon experiments at around 1 TeV and 500 GeV respectively. Recently, Dark Matter Particle Explorer (DAMPE) experiment [34] has also observed a sharp peak around ~ 1.4 TeV favoring the lepto-philic

DM annihilation cross-section of the order of $10^{-26} \text{cm}^3/s$. The excess in e^+e^- can be either due to astrophysical events like high energy emission from the pulsars or resulting from DM pair annihilation in our galactic neighborhood preferably to e^+e^- channel. Since the aforementioned experiments have not observed any significant excess in anti-proton channel, the DM candidates, if any, appears to be lepton friendly *lepto-philic* and have suppressed interaction with quarks at the tree level.

Various UV complete new physics extensions of SM have been proposed essentially to solve the gauge hierarchy problem in the *top-down* approach which include theories like extra-dimensions [35], super-symmetry [36–38], little-Higgs [39, 40], extended 2-HDM models with singlets as portal of DM interactions [41] and *etc.* These models naturally provide the DM candidates or WIMPs, whose mass-scales are close to that of the electro-weak physics. However, the Direct detection experiments have shrunk the parameter space of the simplified and popular models where the WIMPs are made to interact with the visible world *via* neutral scalars and/ or gauge Bosons.

The model independent DM-SM particles interactions have also been studied in the *bottom-up* Effective Lagrangian approach where the mediator of DM-SM interactions are believed to be much heavier than the mass-scale of the lighter degrees of freedom say, in our case SM and DM particles [9–14]. The nature of these interactions are encapsulated in a set of coefficients corresponding to limited number of Lorentz and gauge invariant higher dimensional effective operators constructed with the light degrees of freedom. The constrained parameters (coefficients) space from various experimental data then essentially maps and direct towards the viable UV complete theoretical models. The generic effective Lagrangian for scalar, pseudo-scalar, vector, axial-vector interactions of SM particles with the scalar, vector, spin 1/2 and spin 3/2 dark matter candidates have been studied in literature [42–46].

Sensitivity analysis for DM-quark effective interactions at LHC have been performed in a model-independent way for the dominant (a) mono-jet + \cancel{E}_T , (b) mono- b jet + \cancel{E}_T and (c) mono- t jet + \cancel{E}_T processes [47]. Similarly, analysis for DM-gauge Boson effective couplings at LHC have been done by the authors in reference [48–50]. The sensitivity analysis of the coefficients and detailed analysis of detection cuts flow strategy for lepto-philic operators have also been performed through $e^+e^- \rightarrow \gamma + \cancel{E}_T$ [51–53] and $e^+e^- \rightarrow Z^0 + \cancel{E}_T$ [14, 54] channels.

The effective DM-nucleon scattering induced by twist-2 quark operators are initially studied by the authors of [55] in the context of super-symmetric models where the Majorana DM particle neutralino being LSP was assumed to be much lighter than that of the squark masses. This was followed by series of papers [56–62] where the authors have calculated the one loop effect of DM-nucleon scattering induced by the twist-2 quarks and gluonic operators for the fermion, vector and scalar DM respectively. The hadronic matrix elements induced by twist-2 operators can however be identified with the second moment of parton distribution functions and thus can be constrained from the available *pdfs*. This in turn constrain the coefficients of such higher dimensional effective operators to estimate the DM-nucleon scattering cross-sections for a suggested DM and squark mass range.

In this paper, we undertake the analysis for spin 1/2, 0 and 1 DM interactions in-

duced by *lepto-philic* and $U(1)_Y$ *gauge Boson B-philic* effective twist-2 higher dimensional gauge invariant operators. This article is organised as follows: we formulate the effective interaction Lagrangian for fermionic, scalar and vector DM with SM leptons and neutral electro-weak gauge Bosons *via* twist-2 operators in section 2. In section 3, we constrain the coefficients of the effective Lagrangian from predicted relic density and perform a consistency check *w.r.t.* indirect and direct detection experiments. The constraints from the LEP on the coefficients of the effective lepto-philic and $U(1)_Y$ gauge Boson B-philic operators and the sensitivity analysis of these coefficients at the proposed ILC are discussed in section 4. Finally we summarize in section 5.

2 Effective interactions of lepto-philic & $U(1)_Y$ gauge Boson B-philic DM

We initiate the construction of the effective operators by writing the contact interaction between any SM leptons ψ and fermionic DM χ (Dirac or Majorana) with masses m_ψ and m_χ respectively, assuming that the mediator mass scale, if any, should be of the order of the cut-off of the effective theory ($\sim \Lambda$), which in general is much heavier than the masses of the SM and DM fields. These contact interactions for example can be motivated from the supersymmetric models where spin-independent neutralino-lepton interactions are facilitated by the exchange of heavy sleptons and/ or Higgses, assuming Majorana neutralino to be the LSP. For an illustration of such contact interactions, we write twist-2 Type-1 and Type-2 Lagrangians with the coupling strengths α_1 and α_2 respectively as:

$$\mathcal{L}_1 = \frac{1}{m_\chi} \frac{\alpha_1}{\Lambda^3} (\bar{\chi}\gamma^\mu\partial^\nu\chi) (\bar{\psi}\gamma_\mu\partial_\nu\psi - \partial_\nu\bar{\psi}\gamma_\mu\psi) \quad \text{and} \quad (2.1)$$

$$\mathcal{L}_2 = \frac{1}{m_\chi^2} \frac{\alpha_2}{\Lambda^3} (\bar{\chi}\partial^\mu\partial^\nu\chi) (\bar{\psi}\gamma_\mu\partial_\nu\psi - \partial_\nu\bar{\psi}\gamma_\mu\psi) \quad (2.2)$$

Using the equations of motion for massive Dirac fermions along-with the Tensor identity

$$P_{\mu\nu}Q^{\mu\nu} = (P_{\mu\nu} - \frac{1}{4}g_{\mu\nu}P^\alpha_\alpha)Q^{\mu\nu} + \frac{1}{4}P^\alpha_\alpha Q^\beta_\beta \quad (2.3)$$

the Lagrangians given in equations (2.1) and (2.2) can be re-written as

$$\mathcal{L}'_1 = \frac{1}{m_\chi} \frac{\alpha_1}{\Lambda^3} \left(-2i\mathcal{O}_{\mu\nu}^{(2)}\bar{\chi}\gamma^\mu\partial^\nu\chi - \frac{1}{2}m_\psi m_\chi\bar{\psi}\psi\bar{\chi}\chi \right) \quad \text{and} \quad (2.4)$$

$$\mathcal{L}'_2 = \frac{1}{m_\chi^2} \frac{\alpha_2}{\Lambda^3} \left(-2i\mathcal{O}_{\mu\nu}^{(2)}\bar{\chi}\partial^\mu\partial^\nu\chi - \frac{1}{2}m_\psi m_\chi\bar{\psi}\psi\bar{\chi}\chi \right) \quad (2.5)$$

respectively where $\mathcal{O}_{\mu\nu}^{(2)}$ is defined as trace-less twist-2 operator

$$\mathcal{O}_{\mu\nu}^{(2)} = \frac{i}{2} \left(\bar{\psi}\gamma_\mu\partial_\nu\psi + \bar{\psi}\gamma_\nu\partial_\mu\psi - \frac{g_{\mu\nu}}{2}\bar{\psi}\gamma^\alpha\partial_\alpha\psi \right) \quad (2.6)$$

and $\bar{\psi}\psi\bar{\chi}\chi$ is the scalar operator which has been extensively studied in literature [14, 42]. The twist-2 interactions of fermionic DM can also be realized through the twist-2 operators constructed out of SM electro-weak vector Bosons $\mathcal{O}_{\mu\nu}^{V^{\text{EW}}} \equiv V^{\text{EW}\rho}_\mu V^{\text{EW}}_{\nu\rho} -$

$\frac{1}{4}g_{\mu\nu}V^{\text{EW}}_{\rho\sigma}V^{\text{EW}\rho\sigma}$. Further the formalism can be extended to include the twist-2 Type-2 interactions of spin 0 and spin 1 DM particles with SM charged leptons and electro-weak gauge Bosons using equation (2.5). We analyse all such operators emerging from twist-2 interactions in this study.

We enlist a minimal set of relevant twist-2 lepto-philic and $U(1)_Y$ gauge Boson B-philic operators inducing contact interactions with Dirac fermion χ , real scalar ϕ^0 and real vector V_μ^0 DM candidates in the following Lagrangian:

$$\begin{aligned}\mathcal{L}_{\text{eff. Int.}}^{\text{DM}} &= \mathcal{L}_{\text{eff. Int.}}^{\text{spin } 1/2 \text{ DM}} + \mathcal{L}_{\text{eff. Int.}}^{\text{spin } 0 \text{ DM}} + \mathcal{L}_{\text{eff. Int.}}^{\text{spin } 1 \text{ DM}} \\ &= \sum_{p=l,B} \left[\sum_{T_i \in T_1, T_2} \frac{\alpha_{T_i}}{\Lambda^3} \mathcal{O}_{T_i}^p + \frac{\alpha_S}{\Lambda^2} \mathcal{O}_S^p + \frac{\alpha_V}{\Lambda^2} \mathcal{O}_V^p \right] \\ &= \sum_{p=l,B} \left[\sum_{T_i \in T_1, T_2} \frac{\lambda_{T_i}^\chi{}^2}{\Lambda_{\text{eff}}^3} \mathcal{O}_{T_i}^p + \frac{\lambda_{T_2}^{\phi^0 2}}{\Lambda_{\text{eff}}^2} \mathcal{O}_S^p + \frac{\lambda_{T_2}^{V^0 2}}{\Lambda_{\text{eff}}^2} \mathcal{O}_V^p \right] \quad \text{where,} \quad (2.7a)\end{aligned}$$

$$\mathcal{O}_{T_1}^p = \frac{1}{m_\chi} \bar{\chi} i \partial^\mu \gamma^\nu \chi \mathcal{O}_{\mu\nu}^p \quad (2.7b)$$

$$\mathcal{O}_{T_2}^p = \frac{1}{m_\chi^2} \bar{\chi} i \partial^\mu i \partial^\nu \chi \mathcal{O}_{\mu\nu}^p \quad (2.7c)$$

$$\mathcal{O}_S^p = \frac{1}{m_{\phi^0}^2} \phi^0 i \partial^\mu i \partial^\nu \phi^0 \mathcal{O}_{\mu\nu}^p \quad (2.7d)$$

$$\mathcal{O}_V^p = \frac{1}{m_{V^0}^2} V^{0\rho} i \partial^\mu i \partial^\nu V^0{}_\rho \mathcal{O}_{\mu\nu}^p \quad (2.7e)$$

The twist-2 operators $\mathcal{O}_{\mu\nu}^{l^\pm}$ for charged leptons $l^\pm \equiv e^\pm, \mu^\pm, \tau^\pm$ and $\mathcal{O}_{\mu\nu}^B$ for $U(1)_Y$ gauge field B^μ are defined in terms of the covariant derivative $D_\mu \equiv \partial_\mu + ig' B_\mu$ as

$$\mathcal{O}_{\mu\nu}^{l^\pm} \equiv i \frac{1}{2} \bar{l} \left(D_\mu \gamma_\nu + D_\nu \gamma_\mu - \frac{1}{2} g_{\mu\nu} \not{D} \right) l, \quad (2.8)$$

$$\mathcal{O}_{\mu\nu}^B \equiv B_\mu^\rho B_{\nu\rho} - \frac{1}{4} g_{\mu\nu} B_{\rho\sigma} B^{\rho\sigma}, \quad (2.9)$$

The cut-off scale of the effective theory Λ_{eff} is defined as $(4\pi)^{1/3} \Lambda$ and $\sqrt{4\pi} \Lambda$ for fermionic and Bosonic DM respectively. α_{T_i} and λ_{T_i} are the strengths and couplings of the interactions respectively, where $|\lambda_{T_i}| \leq \sqrt{4\pi}$ and $\Lambda \gtrsim 1$ TeV.

We are now equipped to analyze and constrain these effective interactions from the DM phenomenology.

3 DM Phenomenology

3.1 Constraints from Relic Density

In this sub-section we discuss the relic abundance of *lepto-philic and $U(1)_Y$ gauge Boson-philic* DM and constrain the effective interactions from the predicted DM relic density $\Omega_{\text{DM}} h^2$ of $0.1138 \pm .0045$ and 0.1199 ± 0.0022 by WMAP [7] and Planck [8] collaborations

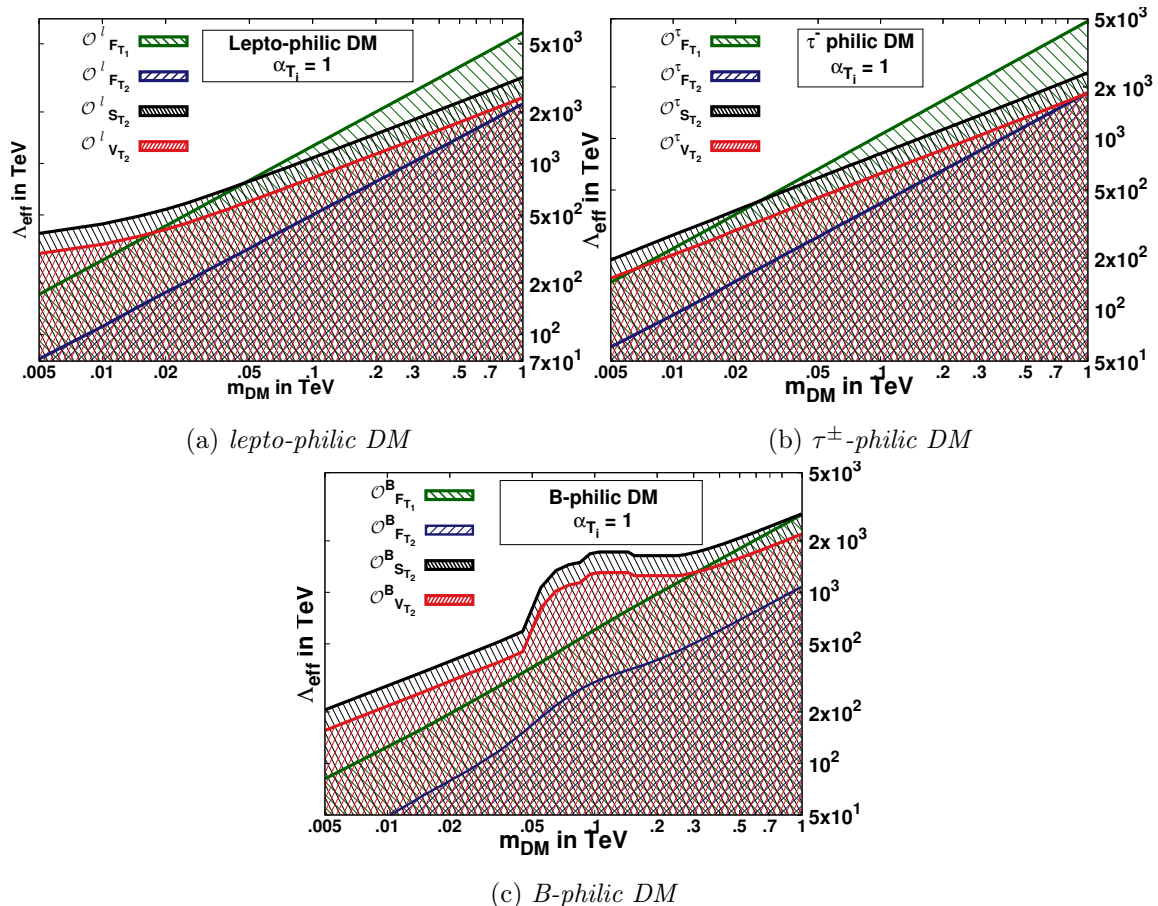


Figure 1: Relic density contours are drawn using *MadDM v.3.0* [63] satisfying $\Omega_{\text{DM}} h^2 = 0.1199 \pm 0.0022$ [8] in the plane defined by DM mass and the respective upper bound on cut-off corresponding to the Type-1 or 2 twist operators operators at fixed coupling $\alpha_{T_i} = 1$. The respective shaded regions depict the allowed parameter space. Contours in figure 1a are depicted assuming the universal lepton flavor couplings of effective DM - SM lepton interactions.

respectively. The current relic density for dark matter is calculated from the DM number density $n_{\text{DM}}(t)$ by solving the Boltzmann equation

$$\frac{d}{dt} n_{\text{DM}}(t) + 3 \mathbf{H}(t) n_{\text{DM}}(t) = - \langle \sigma_{\text{ann}} |\vec{v}| \rangle [n_{\text{DM}}(t)^2 - n_{\text{DM}}^{\text{eq}}(t)^2] \quad (3.1)$$

where \mathbf{H} is the Hubble parameter, $\langle \sigma_{\text{ann}} |\vec{v}| \rangle$ is the thermal average of annihilation cross section multiplied by the relative velocity of dark matter pair. $n_{\text{DM}}^{\text{eq}}$ represents the dark matter number density in thermal equilibrium and is given by $n_{\text{DM}}^{\text{eq}} = \left[\mathbf{g} \left(\frac{m_{\text{DM}} T}{2\pi} \right)^{\frac{3}{2}} \exp \left\{ \frac{-m_{\text{DM}}}{T} \right\} \right]^{1/2}$ where \mathbf{g} is the degrees of freedom. To numerically compute the current DM relic density we need to calculate the thermally averaged DM annihilation cross sections. Since the freeze-out for thermal relics occurs when the massive particle is non-relativistic *i.e.* $|\vec{v}| \ll c$, we make an expansion in $|\vec{v}|/c$ and then $\langle \sigma |\vec{v}| \rangle$ can be approximated as $\langle \sigma |\vec{v}| \rangle = a + b |\vec{v}|^2 + \mathcal{O}(|\vec{v}|^4)$.

Defining the dark matter relic abundance as a ratio of the thermal relic density ρ_{DM} and critical density of the universe $\rho_c = 1.05373 \times 10^{-5} \mathbf{h}^2 \text{ GeV}/(c^2 \text{ cm}^3)$, where \mathbf{h} is the dimensionless Hubble parameter and solving the Boltzmann equation for the thermal relic density we get

$$\begin{aligned} \Omega_{\text{DM}} \mathbf{h}^2 &= \frac{\pi \sqrt{\mathbf{g}_{\text{eff}}(x_F)}}{\sqrt{90}} \frac{x_F T_0^3 \mathbf{g}_0}{M_{\text{Pl}} \rho_c \langle \sigma_{\text{ann}} v \rangle \mathbf{g}_{\text{eff}}(x_F)} \\ &\approx 0.12 \frac{x_F}{28} \frac{\sqrt{\mathbf{g}_{\text{eff}}(x_F)}}{10} \frac{2 \times 10^{-26} \text{ cm}^3/\text{s}}{\langle \sigma |\vec{v}| \rangle} \end{aligned} \quad (3.2)$$

where M_{Pl} and \mathbf{g}_{eff} are Planck mass and effective number of degrees of freedom near the freeze-out temperature $T_F = \frac{m_{\text{DM}}}{x_F}$, where x_F is given by

$$x_F = \log \left[c' (c' + 2) \sqrt{\frac{45}{8}} \frac{\mathbf{g}_0 M_{\text{Pl}} m_{\text{DM}} \langle \sigma |\vec{v}| \rangle}{2 \pi^3 \sqrt{x_F \mathbf{g}_{\text{eff}}(x_F)}} \right] \quad (3.3)$$

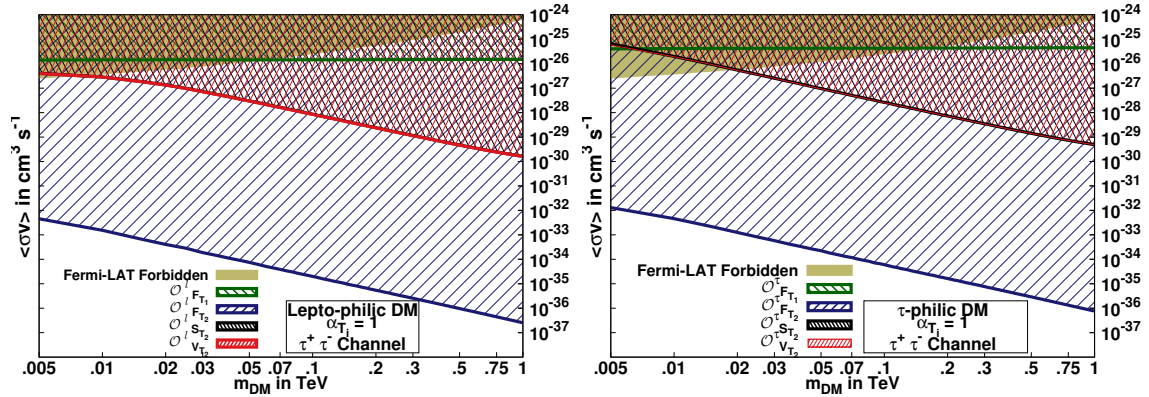
where c' is a parameter of the order of one.

We have computed the thermal-averaged annihilation cross-section in the appendix for the Dirac fermion, a real scalar and real vector DM candidates. They are worked out in the Appendix A. For τ^\pm -philic (electro-philic) case, all DM - leptons couplings except that of DM - τ^\pm (e^\pm) identically vanish.

To compute relic density numerically, we have used MadDM [63] and MadGraph [64]. We have generated the input model file required by MadGraph using FeynRules [65], which calculates all the required couplings and Feynman rules by using the full Lagrangian given in equation (2.7). We scan over the DM mass range 10 - 1000 GeV whose relic density satisfy $\Omega_{\text{DM}} \mathbf{h}^2 \leq 0.1199$ [8] for all vanishing interactions except one non-zero coupling α_{T_i} fixed at unity. We study and plot the relic density contours in the plane defined by DM mass and the cut-off corresponding to four (two fermionic, one scalar and one Vector DM) lepto-philic, τ^\pm -philic and B -philic operators in figures 1a, 1b and 1c respectively. All points lying on the solid lines in figure 1 satisfy $\Omega_{\text{DM}} \mathbf{h}^2 \leq 0.1199$ [8]. These points are also the allowed upper limit on the cut-off for a given DM mass and thus the shaded region enclosed by the corresponding solid line is the cosmologically allowed parameter region of the respective operator. The lower value of the cut-off corresponding to the same DM mass will lead to only partial contribution to relic density and therefore may survive in model where (a) more than one type of DM particles are allowed and/ or (b) switching more than one type of effective operators simultaneously. We observe that the sensitivity of the cut-off for fermionic Type-1 operator increases with the varying DM mass. Among the Type-2 operators, scalar DM cut-off is found to be the most sensitive. It is important to mention that the relic density contours for a electro-philic DM will be almost same to that of the τ^\pm -philic case.

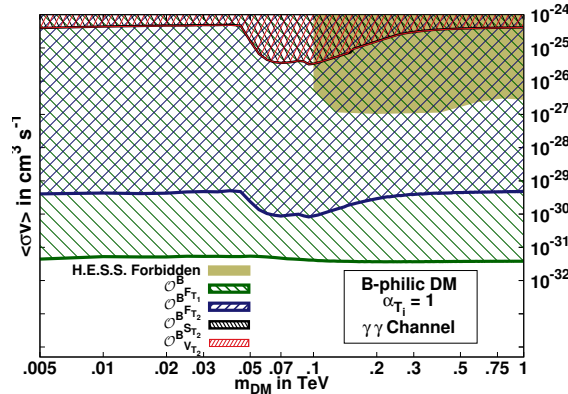
3.2 Indirect Detection

Since the DM annihilation rate is proportional to the square of DM density, therefore DM annihilation is likely to be propelled in the over-dense region of the universe such as



(a) Lepto-philic DM annihilation to $\tau^+\tau^-$

(b) τ^\pm -philic DM DM annihilation to $\tau^+\tau^-$



(c) B-philic DM annihilation to $\gamma\gamma$

Figure 2: Solid lines in all figures depict the variation of thermally averaged DM annihilation cross-sections w.r.t. the DM mass at the fixed coupling $\alpha_{T_i} = 1$ and the respective upper bound on the cut-off satisfying the relic density contribution. We plot the median of the DM annihilation cross section derived from a combined analysis of the nominal target sample for the $\tau^+\tau^-$ channel [26] in figures 2a, 2b and $\gamma\gamma$ [27] channel in figure 2c assuming a 100% branching fraction and thus restrict the respective allowed shaded region from above. Figure 2a shows the contours for the fermionic, scalar and vector DM interacting via Type-1 or 2 twist operators assuming the universal lepton flavor couplings with the DM.

galactic center, dwarf spheroids and sun generate high flux of energetic light SM particles like charged hadrons, jets, the charged leptons *e.g.* electron, positron and photon. Since the non-relativistic DM particles are colliding at rest with each other, the energy of gamma-rays and the produced charged lepton is of the order of $\sim m_{\text{DM}}$. Indirect experiments which in general are either ground-based or satellite borne particle detectors are sensitive to these characteristic fluxes of light SM particles. For example FermiLAT (Large Area Telescope) is a space borne experiment designed to measure the tracks of electron-positron pairs which are produced when gamma-rays interact with the detector material (thin and high-Z foil) [24–26], while HESS is the ground based cherenkov telescope geared to detect the gamma ray spectrum [27].

In this section we calculate the thermally averaged annihilation cross sections for

fermionic, real scalar and real vector Boson DM candidates to pair of charged leptons and photons. The analytical expressions for these cross-sections corresponding to the lepto-philic and $U(1)_Y$ gauge Boson B-philic operators are given in equations (A.10)-(A.13) and (A.14)-(A.17) respectively. We have used 220 Km/s (average rotational velocity of galaxy) as the average velocity of the DM.

The thermal averaged DM annihilation cross-section is computed numerically for a given set of parameter ($m_{\text{DM}}, \alpha_{T_i}, \Lambda_{\text{eff}}$) which satisfy the relic density constraint from the Planck data as depicted in figure 1. For the lepto-philic and τ^\pm -philic operators we compute the dominant thermal averaged annihilation cross-section to $\tau^+\tau^-$ pair using equations (A.10), (A.11), (A.12) and (A.13) corresponding to the fermionic DM Type-1 and Type-2, scalar DM Type-2 and vector DM Type-2 induced operators. The variation of the annihilation cross-section with the DM mass are depicted in figures 2a and 2b respectively. The solid lines in figures 2a and 2b are essentially the lower bound on the allowed annihilation cross-section satisfying the relic density constraints for a given DM mass. It is interesting to note that although the analytical expression for the scalar and vector DM annihilation cross-section are not same but still we observe a complete overlap of the scalar and vector DM solid lines for $\alpha_{T_2}^{V^0} = \alpha_{T_2}^{\phi^0}$ which is an artifact of the two distinct values of the respective effective cut-off that satisfy the same relic density for a given DM mass. These results are compared with the upper bound on the allowed annihilation cross-section in $\tau^+\tau^-$ channel obtained from the FermiLAT data [26]. Thus the null experimental results for the given mass range translate into the lower limits on the cut-off for the respective operators. The DM annihilation cross-section to the pair of electrons induced by the electro-philic DM are identical to those depicted in figure 2b for the respective operators.

For $U(1)_Y$ gauge Boson B-philic DM, we look for the photon pair production channel and the thermally averaged DM annihilation cross section is computed using equations (A.14), (A.15), (A.16) and (A.17) corresponding to the fermionic DM Type-1 and 2, scalar DM and vector DM Type-2 induced operators respectively. Figure 2c show the allowed shaded region for annihilation cross-sections with the points on the solid line for each case satisfying the relic density and thereby giving the lower bound on the cosmologically allowed annihilation cross-section. As in the case of lepto-philic and τ^\pm -philic, we observe that the scalar and vector annihilation cross-section overlaps for the reason mentioned earlier. We compare our results with that obtained from the null observation at HESS [27] for DM mass 100 GeV and above, which

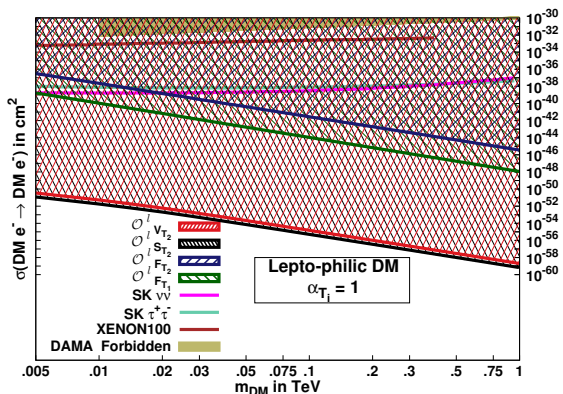


Figure 3: Variation of DM - free electron elastic scattering cross-sections w.r.t. the DM mass at fixed lepton flavor universal coupling $\alpha_{T_i} = 1$ and the respective upper bound on the cut-off satisfying the relic density contribution for lepto-philic operators. The exclusion plots from DAMA at 90% C.L. for the case of DM-electron scattering are also shown [66]. Bounds at 90% C.L. are shown for XENON100 from inelastic DM-atom scattering [67]. The dashed curves show the 90% CL constraint from the Super-Kamiokande limit on neutrinos from the Sun, by assuming annihilation into $\tau^+\tau^-$ or $\nu\bar{\nu}$ [66].

gives the upper lower bounds on the respective B-philic operators.

3.3 DM-electron scattering

Direct detection experiments [15–23] look for the scattering of nucleon or atom by DM particles. These experiments are designed to measure the recoil momentum of the nucleons or atoms of the detector material. These scattering can be broadly classified as (a) DM-electron scattering, (b) DM-atom scattering, and (c) DM-nucleus scattering. Since the lepto-philic, τ^\pm -philic and B-philic DM do not have direct interactions with quarks or gluons at tree level. therefore we explore tree level DM-electron elastic scattering induced by the lepto-philic operators only. We consider scattering of the non-relativistic DM by the free electron at rest induced by lepto-philic operators at tree level and avoid the complications arising due to the bound electrons and keep in mind that such detailed calculation will give us a further suppression factor of the order of $\sim 10^{-6}$ as explicitly shown in reference [66].

The DM - free electron scattering cross-sections for the fermion DM with Type-1 and 2 lepto-philic twist-2 operators are computed and given as

$$\sigma_{T1}^{\chi e} = 36\pi\alpha_{T1}^2 \frac{m_e^4}{\Lambda_{\text{eff}}^6} \quad (3.4a)$$

$$\sigma_{T2}^{\chi e} = 36\pi\alpha_{T2}^2 \frac{m_e^4}{\Lambda_{\text{eff}}^6} \quad (3.4b)$$

Similarly, the analytical expression for the DM-electron scattering cross-section corresponding to Type-2 scalar and vector twist-2 lepto-philic operators are given as

$$\sigma_{T2}^{\phi^0 e} = 9\pi \frac{\alpha_{\phi^0}^2}{\Lambda_{\text{eff}}^4} \frac{m_e^4}{m_{\phi^0}^2} \quad (3.5a)$$

$$\sigma_{T2}^{V^0 e} = 9\pi \frac{\alpha_{V^0}^2}{\Lambda_{\text{eff}}^4} \frac{m_e^4}{m_{V^0}^2} \quad (3.5b)$$

In figure 3 we plot the DM - free electron elastic scattering cross-section with varying DM mass depicted in solid lines for Fermionic Type-1 and 2, scalar Type-2 & vector Type-2 twist-2 lepto-philic operators. The cross-section is computed for the coupling fixed at the unity and the corresponding cut-off which satisfy the relic density $\Omega_{\text{DM}}h^2 = 0.119$ [8] for a given DM mass. Although the analytical expressions of the scattering processes for the scalar and vector DM are similar but we observe the two distinct solid lines corresponding to these contributions in figure 3 because of the respective values of the cut-off contributing to the same relic density for a given DM mass when $\alpha_{T2}^{V^0} = \alpha_{T2}^{\phi^0}$. These results are then compared with the null results of DAMA/LIBRA [15, 16] at 90% confidence level for DM-electron scattering and XENON100 [20, 21] at 90% confidence level for inelastic DM-atom scattering. The shaded region bounded between the solid line corresponding to each operator and the null result of the experimental bound translate into allowed region in parameter space of the model for a given DM mass.

It is important to note that electro-philic DM -free electron scattering cross-sections corresponding to the respective operators computed using the upper bound on the cut-off

obtained for a given DM mass from relic density constraints as shown in figure 1b and unity coupling strength, will be slightly higher than those shown in the figure 3. The DM - free electron scattering corresponding to the τ^\pm -philic and B-philic operators occurs at the one loop level and therefore are further suppressed.

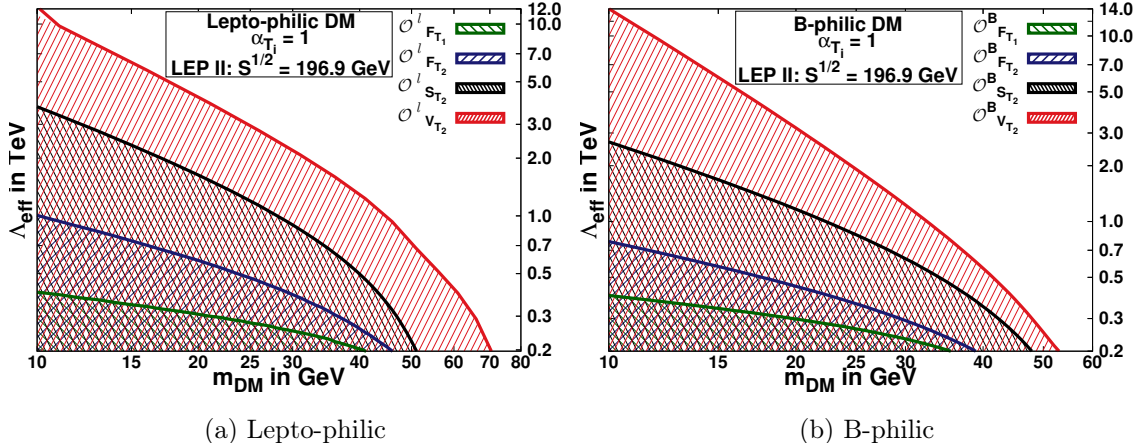


Figure 4: Solid lines depict the contours in the plane defined by DM mass and the kinematic reach of the cut-off Λ_{eff} for $e^+e^- \rightarrow \text{DM pairs} + \gamma^* \rightarrow \cancel{E}_T + q_i\bar{q}_i$ at fixed coupling $\alpha_{T_i} = 1$, $\sqrt{s} = 196.9$ GeV and an integrated luminosity of 679.4 pb^{-1} , satisfying the constraint $\delta\sigma_{\text{tot}} = .032 \text{ pb}$ obtained from combined analysis of DELPHI and L3 [68]. The enclosed shaded region corresponding to each solid line are forbidden by LEP observation.

4 Collider sensitivity of effective operators

4.1 LEP Constraints on the effective operators

We investigate the constraints on the lepto-philic and B-philic effective operators from the existing results and observations from LEP data. We compute the cross-section for the process $e^+e^- \rightarrow \gamma^* + \text{DM pair}$, and compare with the combined analysis from DELPHI and L3 collaborations for $e^+e^- \rightarrow \gamma^* + Z \rightarrow q_i\bar{q}_i + \nu_{l_j}\bar{\nu}_{l_j}$ at $\sqrt{s} = 196.9$ GeV and an integrated luminosity of 679.4 pb^{-1} , where $q_i \equiv u, d, s$ and $\nu_{l_j} \equiv \nu_e, \nu_\mu, \nu_\tau$. The measured cross-section from the combined analysis for the said process is found to be $.055 \text{ pb}$ along with the measured statistical error $\delta\sigma_{\text{stat}}$, systematic error $\delta\sigma_{\text{syst}}$ and total error $\delta\sigma_{\text{tot}}$ of $.031 \text{ pb}$, $.008 \text{ pb}$ and $.032 \text{ pb}$ respectively [68]. Therefore, contribution due to an additional channel containing the final states DM pairs and resulting into the missing energy along with two quark jets can be constrained from the observed $\delta\sigma_{\text{tot}}$.

In figures 4a and 4b, we plot the 95% C.L. solid line contours satisfying the cross-section observed $\delta\sigma_{\text{tot}} .032 \text{ pb}$ corresponding to the lepto-philic and B-philic operators in the two dimensional plane defined by the DM mass and the lower bound on the cut-off at the fixed value of respective coupling α_{T_i} . The respective shaded regions in figure 4 are disallowed by the combined LEP analysis. Thus the phenomenologically interesting DM mass range $\lesssim 50 \text{ GeV}$ is completely disfavored by the LEP experiments.

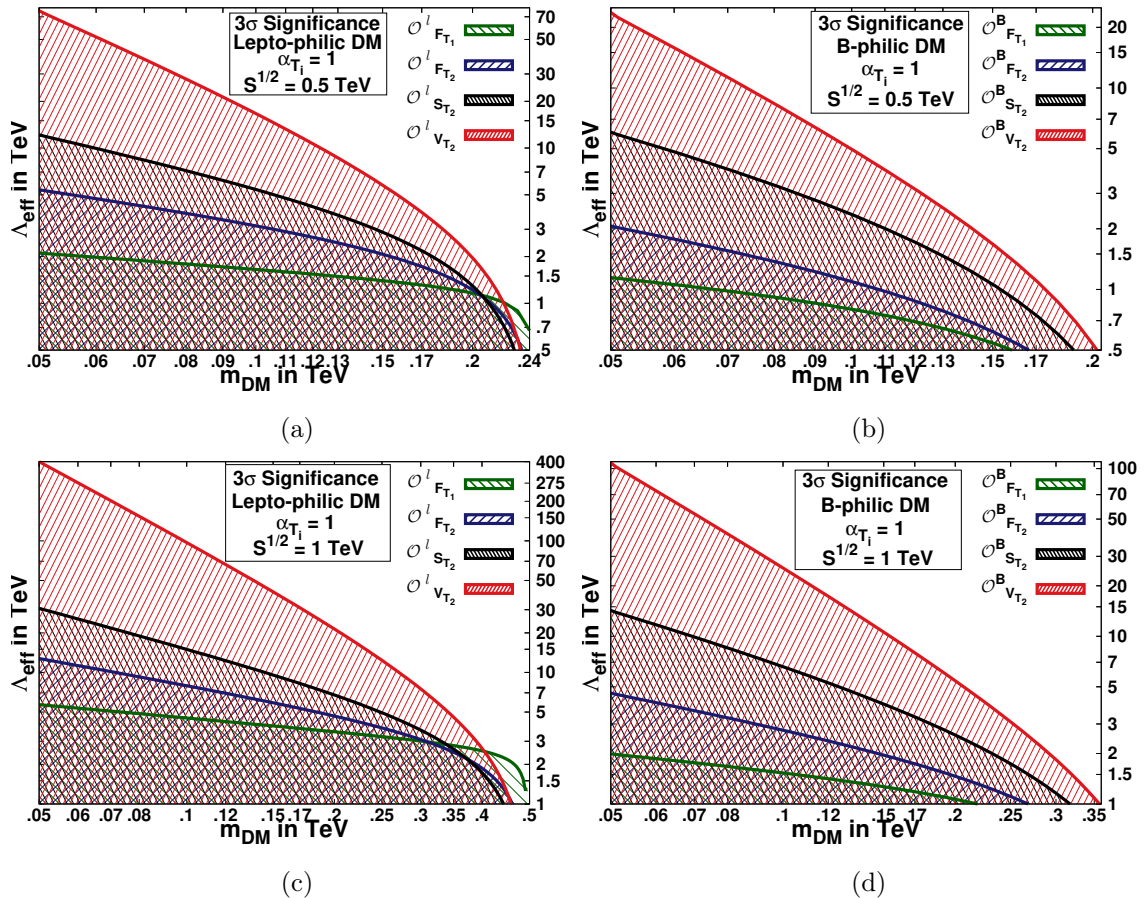


Figure 5: Solid lines depict 3σ efficiency contours at fixed coupling $\alpha_{T_i} = 1$ for DM pair production process with mono-photon ($e^+e^- \rightarrow \cancel{E}_T + \gamma$) in the plane defined by DM mass and the kinematic reach of the cut-off Λ_{eff} corresponding to (a) $\sqrt{s} = 500$ GeV; $\mathcal{L} = 500 \text{ fb}^{-1}$ in 5a and 5b and (b) $\sqrt{s} = 1$ TeV; $\mathcal{L} = 1 \text{ ab}^{-1}$ in 5c and 5d. The shaded region corresponding to each solid line are likely to be probed by ILC with greater than 3σ efficiency.

	ILC-500	ILC-1000
\sqrt{s} (in GeV)	500	1000
\mathcal{L}_{int} (in fb^{-1})	500	1000
σ_{bg} (pb)	1.48	2.07

Table 1: Accelerator parameters as per Technical Design Report [71, 72]. σ_{bg} is the background cross section for $e^-e^+ \rightarrow \sum \nu_i \bar{\nu}_i \gamma$ process computed using the selection cuts defined in section 4.2

4.2 $\cancel{E}_T + \text{Mono-photon}$ signals at ILC

We consider following DM production processes along with mono-photon at the proposed ILC for the DM mass range $\sim 50 - 500$ GeV: (a) $e^+e^- \rightarrow \chi \bar{\chi} \gamma$, (b) $e^+e^- \rightarrow \phi^0 \phi^0 \gamma$, and (c) $e^-e^- \rightarrow V^0 V^0 \gamma$. The dominant SM background for $e^+e^- \rightarrow \cancel{E}_T + \gamma$ signature comes from $Z^0 \gamma$ production process: $e^-e^+ \rightarrow Z^0 + \gamma \rightarrow \sum \nu_i \bar{\nu}_i + \gamma$. The analysis for background and signal processes with certain choices of the accelerator parameters as conceived in the

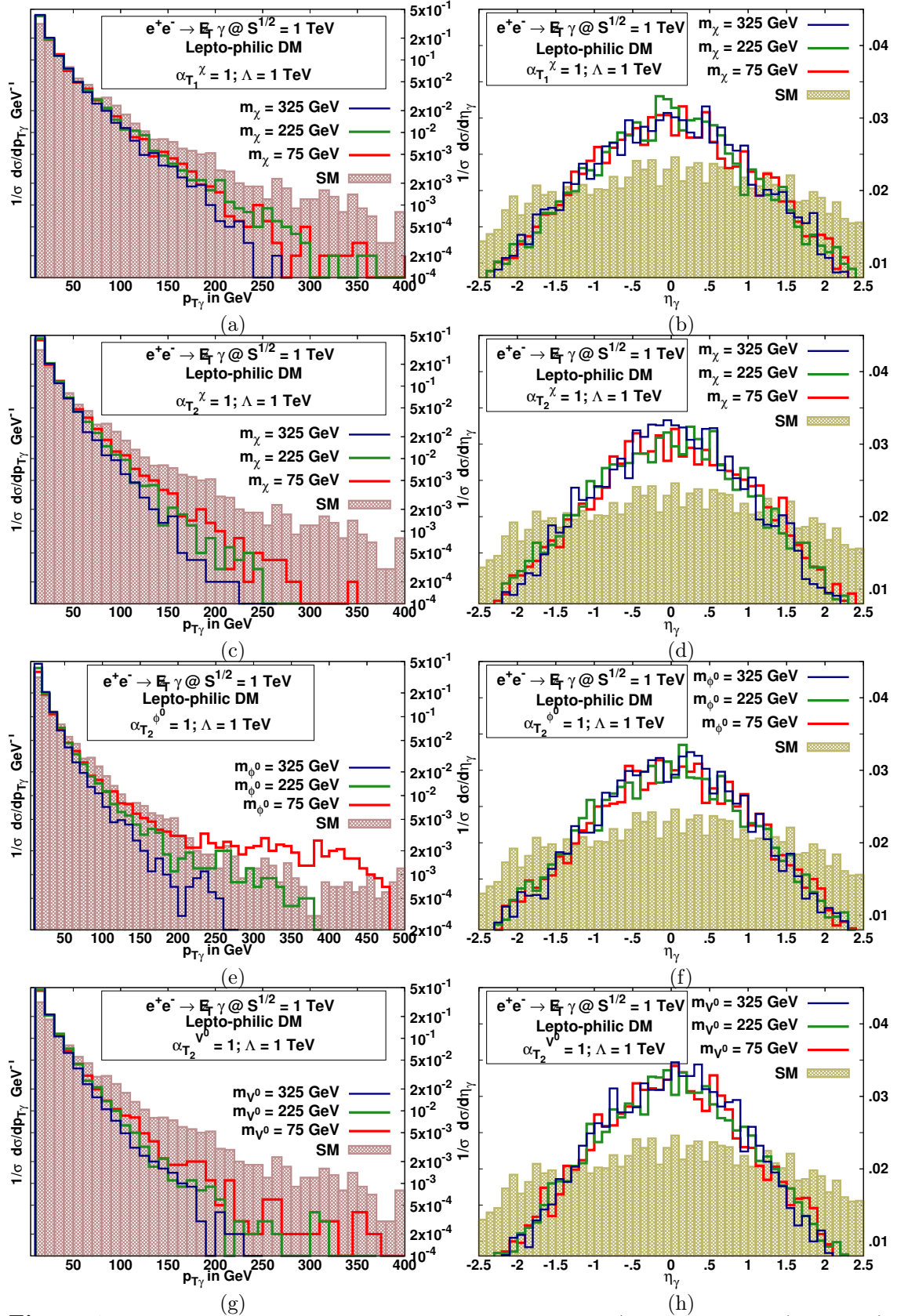


Figure 6: Normalized 1-D differential cross-sections w.r.t. p_{T_γ} (bin width 10 GeV) and η_γ (bin width 0.1) corresponding to the SM processes (shaded histograms) and those induced by lepto=philic operators at the three representative values of DM masses: 75, 225 and 325 GeV respectively.

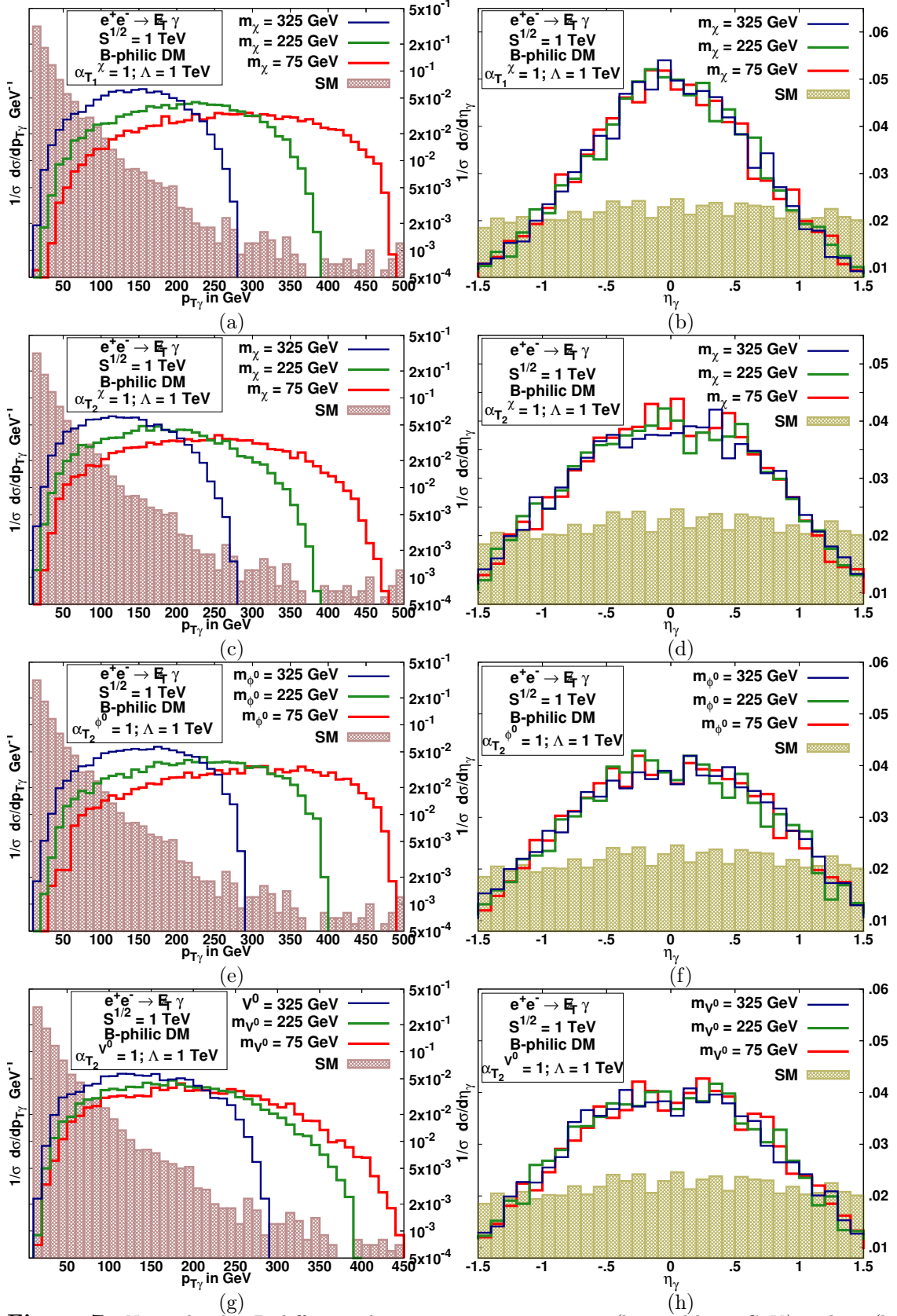


Figure 7: Normalized 1-D differential cross-sections w.r.t. p_{T_γ} (bin width 10 GeV) and η_γ (bin width 0.1) corresponding to the SM processes (shaded histograms) and those induced by B-philic operators at the three representative values of DM masses: 75, 225 and 325 GeV respectively.

Technical Design Report for ILC [71, 72] and given in Table 1 are performed by simulating SM backgrounds and the DM signatures using Madgraph [64] and the model file generated by FeynRules [65]. The basic selection cuts applied to reduce the SM background for this analysis are as follows [53]:

- Transverse momentum of photon $p_{T_\gamma} \geq 10$ GeV,
- Pseudo-rapidity of photon is restricted as $|\eta_\gamma| \leq 2.5$,
- Emerging angle of photon is restricted to avoid IR singularities by imposing the cut on the allowed photon energy $2 E_\gamma/\sqrt{s} \in [0.95, 0.98]$ and $[0.98, 0.99]$ for $\sqrt{s} = 500$ and 1 TeV respectively.

As a first step towards preliminary analysis we study the significance \mathcal{S} for the DM production processes, defined as

$$\mathcal{S} = \frac{N_S}{\sqrt{N_B + (\delta_{\text{sys}} N_B)^2}} \quad (4.1)$$

where N_S is the number of DM with mono-photon events, N_B is the number of SM background events and δ_{sys} is the systematic error. The 3σ sensitivity contours in $\Lambda_{\text{eff}} - m_{\text{DM}}$ plane are drawn for the DM production cross-sections with $\alpha_{T_i} = 1$ and conservative $\delta_{\text{sys}} \sim 1\%$ in figures 5a, 5b, 5c and 5d. Figures 5a and 5b correspond to lepto-philic and B-philic operators respectively for the proposed ILC at $\sqrt{s} = 500$ GeV at an integrated luminosity of 500 fb^{-1} , while figures 5c and 5d respectively depict the same for $\sqrt{s} = 1$ TeV at an integrated luminosity of 1 ab^{-1} . The shaded region of parameter space associated with each contour can be explored by the proposed collider at $\mathcal{S} \geq 3$. Thus, we get the kinematic reach on the cut-off scale Λ_{eff} at ILC for all relevant twist-2 lepto-philic and $U(1)_Y$ gauge Boson B-philic induced DM operators.

4.3 Differential Cross-sections and χ^2 Analysis

The photon transverse momentum (p_{T_γ}) and photon pseudo-rapidity (η_γ) are found to be sensitive kinematic observables for the process $e^+e^- \rightarrow \cancel{E}_T + \gamma$. We generate the one dimensional distribution for the SM background processes and signals for the fermionic, real scalar and real vector DM candidates, keeping only one effective coupling constant as defined in equation (2.7) to be non-zero. To study the shape profile and its mass dependence, we plot the normalized differential cross-sections *w.r.t.* p_{T_γ} and η_γ induced by Type-1 lepto-philic twist-2 operator in figures 6a and 6b respectively keeping $\alpha_{T_1}^X = 1$ and all other $\alpha_{T_2}^{X^{V^0, \phi^0}} = 0$ and $\Lambda_{\text{eff}} = 1$ TeV. Similarly, keeping one coupling at a time to be unity and for fixed $\Lambda_{\text{eff}} = 1$ TeV we draw the normalized differential distributions for fermionic, scalar and vector Type-2 lepto-philic twist-2 DM operators *w.r.t.* p_{T_γ} in figures 6c, 6e and 6g respectively and *w.r.t.* η_γ in figures 6d, 6f and 6h respectively. Each figure depict three shape profiles of the differential distribution corresponding to three choices of DM masses 75, 225 and 325 GeV respectively. Shaded golden yellow histograms depict the normalized

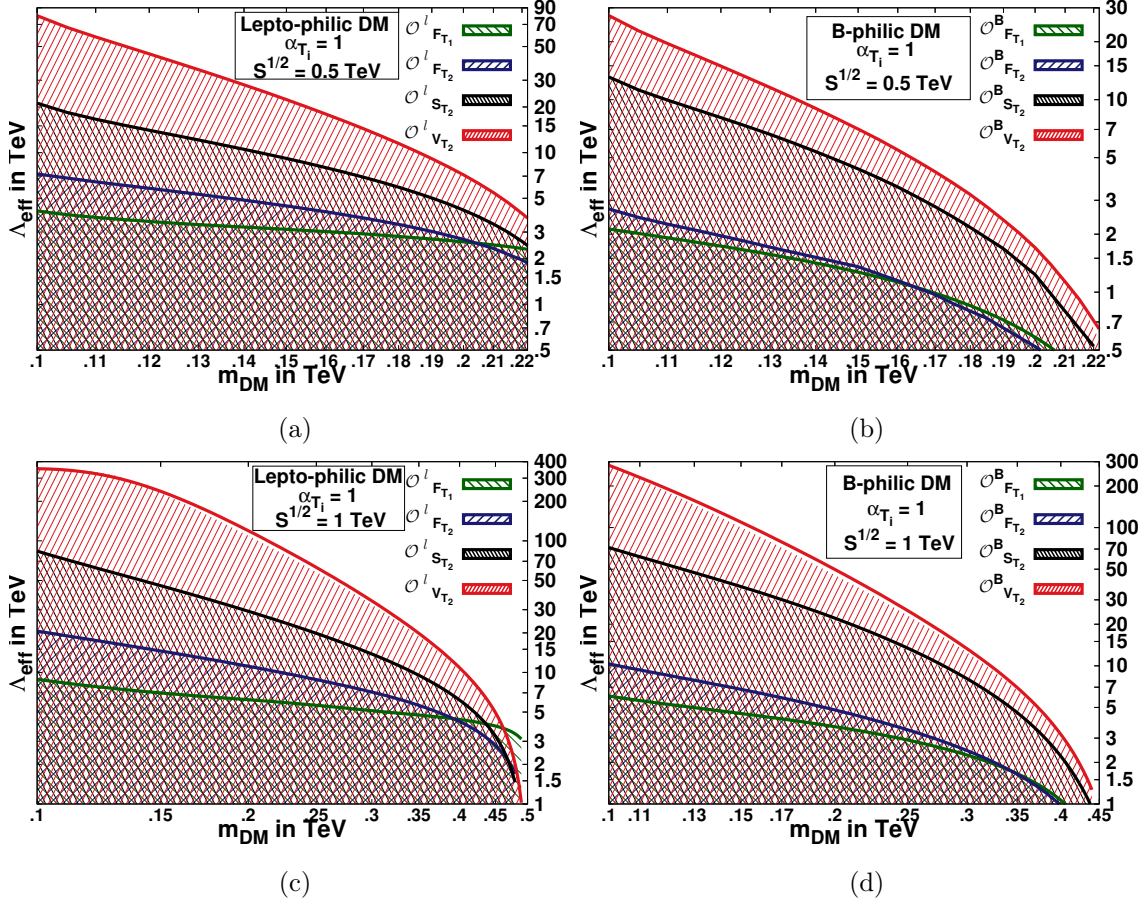


Figure 8: Solid lines depict 3σ with 99.73 % C.L. contours in the $m_{\text{DM}} - \Lambda_{\text{eff}}$ plane from the χ^2 analyses of the $e^+e^- \rightarrow \cancel{E}_T + \gamma$ signature at the proposed ILC designed for (a) $\sqrt{s} = 500$ GeV with an integrated luminosity 500 fb^{-1} in figures 8a & 8b, and (b) $\sqrt{s} = 1$ TeV with an integrated luminosity 1 ab^{-1} in figures 8c & 8d respectively. Each figure contain four contours corresponding to the twist-2 Type-1 fermionic & Type-2 fermionic, scalar and vector operators respectively. The enclosed shaded region corresponding to the respective contour is accessible for discovery with $\geq 99.73\%$ C.L.

differential distributions *w.r.t.* p_{T_γ} in figures 6a, 6c, 6e, 6g and *w.r.t.* η_γ in figures 6b, 6d, 6f, 6h respectively for the background processes.

Repeating the same exercise for the B-philic operators, we depict the shape profile of the normalised differential distribution corresponding to three choices of DM masses 75, 225 and 325 GeV induced by Type-1 fermionic, Type-2 fermionic, scalar and vector DM *w.r.t.* p_{T_γ} in figures 7a, 7c, 7e, 7g and *w.r.t.* η_γ in figures 7b, 7d, 7f, 7h respectively. The respective differential distribution for the background SM processes are depicted in all of these figures and are shown in shaded golden yellow histograms.

We note that $p_{T_\gamma}^{\text{max}}$ decreases with increase in DM mass. The shape of normalized distributions are comparatively more sensitive *w.r.t.* DM masses in case of the B-philic operators. This suggests that for the B-philic operators induced interactions, imposition of DM mass

dependent dynamical cut can minimize the background and enhance the significance.

However, to enhance the sensitivity of the Λ_{eff} at a fixed coupling $\alpha_{T_i} = 1$ *w.r.t.* DM masses, we compute the χ^2 with the double differential distributions of kinematic observables p_{T_γ} and η_γ corresponding to the background and signal processes for (a) $100 < m_{\text{DM}} < 250$ GeV at $\sqrt{s} = 500$ GeV and an integrated luminosity of 500 fb^{-1} , and (b) $100 < m_{\text{DM}} < 500$ GeV at $\sqrt{s} = 1$ TeV and an integrated luminosity of 1 ab^{-1} . The χ^2 is defined as

$$\chi^2 \equiv \chi^2(m_{\text{DM}}, \alpha_{T_i}, \Lambda_{\text{eff}}) = \sum_{j=1}^{n_1} \sum_{i=1}^{n_2} \left[\frac{\frac{\Delta N_{ij}^{NP}}{(\Delta p_{T_\gamma})_i (\Delta \eta_\gamma)_j} (m_{\text{DM}}, \alpha_{T_i}, \Lambda_{\text{eff}})}{\sqrt{\frac{\Delta N_{ij}^{SM+NP}}{(\Delta p_{T_\gamma})_i (\Delta \eta_\gamma)_j} (m_{\text{DM}}, \alpha_{T_i}, \Lambda_{\text{eff}}) + \delta_{\text{sys}}^2 \left\{ \frac{\Delta N_{ij}^{SM+NP}}{(\Delta p_{T_\gamma})_i (\Delta \eta_\gamma)_j} (m_{\text{DM}}, \alpha_{T_i}, \Lambda_{\text{eff}}) \right\}^2}} \right]^2 \quad (4.2)$$

where ΔN_{ij}^{NP} and ΔN_{ij}^{SM+NP} are the number of differential New Physics and total events respectively in the two dimensional $\left[(\Delta p_{T_\gamma})_i - (\Delta \eta_\gamma)_j \right]^{\text{th}}$ grid. Here δ_{sys} represents the total systematic error in the measurement.

We consider only one effective operator at time with the fixed coupling constant of unity and adopted a conservative value for the systematic error to be 1%. We simulate the two-dimension differential distributions using the collider parameters as given in Table 1 and choosing the basic selection cuts. In addition we impose DM mass dependent dynamical cuts to minimize the background for $U(1)_Y$ gauge Boson B-philic induced interactions, which translates into an acceptance dynamical cut on the photon energy

$$E_\gamma \leq \frac{s - 4m_{\text{DM}}^2}{2\sqrt{s}}. \quad (4.3)$$

We plot the 3σ contours at 99.73% C.L. in the $m_{\text{DM}} - \Lambda_{\text{eff}}$ for lepto-philic and B-philic operators in figures 8a and 8b respectively corresponding to $\sqrt{s} = 500$ GeV with an integrated luminosity of 500 fb^{-1} . We also give the 3σ contours at 99.73% C.L. for an upgraded high luminosity ILC operating at $\sqrt{s} = 1$ TeV with an integrated luminosity of 1 ab^{-1} in figures 8c and 8d corresponding to interactions induced by lepto-philic and B-philic operators respectively.

We observe that the kinematic reach of the Λ_{eff} is enhanced 5-6 times in comparison to that obtained from the naive significance analysis. The B-philic operators showed better response to the χ^2 analysis based on the double differential distributions which was expected from their one dimensional distribution shown in figure 7.

5 Summary and Outlook

The recent constraints derived from the observation on the dwarf spheroidal satellite galaxies in Fermi-LAT [24–26], excess in electron/positron channel around 10 GeV at PAMELA

[30, 31], excess in flux of electrons/positrons around 400-500 GeV at ATIC [32] and PPB-BETS [33] balloon experiments and exclusion of quark channels by AMS-02 data [28, 29] hints toward the existence of non-baryonic DM. This implies that the direct detection experiments have to be sensitive on the recoil momentum of the atom or an electron in DM - atom and/ or DM - electron scattering respectively due to suppressed loop-level interactions of DM with the quarks in the nucleon. Characterization for such lepto-philic and electro-weak gauge Boson B-philic DM particles are likely to be difficult and challenging at the LHC and therefore it becomes imperative to probe the sensitivity of the associated DM pair production channels at the proposed lepton collider ILC. Motivated by these observations and restrictions, we have explored the viable alternative stable non-baryonic spin 1/2, 0 and 1 DM particles $\sim 10 - 1000$ GeV, contributing to the relic density through their super-weak interactions with twist-2 leptonic and $U(1)_Y$ gauge Boson currents in a model independent approach. In this article, we have considered the super-symmetric models inspired effective second rank twist interactions of the leptons and gauge Bosons with the spin 1/2, 0 and 1 DM candidates.

We have listed a minimal set of the twist-2 operators corresponding to lepto-philic and $U(1)_Y$ gauge Boson tensor currents in section 2 which couples to the tensor currents generated by the bi-linears of the DM fields.

We have analytically calculated the thermalized annihilation cross-sections for the fermionic, scalar and vector DM induced by lepto-philic (A.10) - (A.13) and B-philic (A.14) - (A.17) operators respectively, which are in agreement numerically with that of MadDM. The relic density contours satisfying the PLANCK observations depict the upper bound on Λ_{eff} for fixed coupling $\alpha_{T_i} = 1$ in the $m_{\text{DM}} - \Lambda_{\text{eff}}$ as shown in figures 1a, 1b and 1c for the lepto-philic, τ^\pm -philic and B-philic DM interactions respectively. Using these upper bounds on Λ_{eff} for a given m_{DM} , we estimated the thermally averaged annihilation indirect detection cross-section for lepto-philic and τ^\pm -philic or electro-philic in figures 2a and 2b respectively are compared with that obtained from Fermi-LAT [24-26], while thermally averaged annihilation indirect detection cross-section for B-philic DM shown in figure 2c is compared with the observations from H.E.S.S. data [27]. We find that the present experimental limits in the respective searches not only favours the allowed parameter space from the relic density, but also constraints the DM model by providing the lower bound on the $\Lambda_{\text{eff min}}$ for a given DM mass at fixed coupling α_{T_i} .

We have computed the elastic DM - free electron direct detection scattering cross-section analytically only for lepto-philic induced interactions and depicted in figure 3 as the τ^\pm -philic and B-philic DM interactions do not have any tree level interactions either with the atom or the nucleon. Although the contribution of the loops are suppressed but they need to be investigated for the complete study of the twist-2 operators. On superimposing inelastic DM - atom scattering cross-section from DAMA [66]. XENON100T [67] we observe that the parameter space allowed by the relic density is shrunk and we get a conservative lower limit on the cut-off at fixed coupling $\alpha_{T_i} = 1$ for a given DM mass.

Next, we probed the smoking gun signature in the process $e^+e^- \rightarrow \cancel{E}_T + \gamma$ at ILC induced through twist-2 interactions of lepto-philic and B-philic interactions for $m_{\text{DM}} \sim 50 - 400$ GeV. The 3σ significance contours for the DM pair production in association with

mono-photon at 99.73% C.L. are drawn *w.r.t.* SM background in figures 5a and 5b for lepto-philic and B-philic respectively at $\sqrt{s} = 500$ GeV and an integrated luminosity of 500 fb⁻¹ and in figures 5c and 5d respectively for $\sqrt{s} = 1$ TeV and 1 ab⁻¹, with basic kinematic cuts in Table 1. We improve the sensitivity of the Λ_{eff} by minimizing the χ^2 using the optimal variable technique on the 2-D distributions *w.r.t.* p_{T_γ} and η_γ for the two stages of the proposed collider (i) at $\sqrt{s} = 500$ GeV with an integrated luminosity of 500 fb⁻¹ and (ii) at $\sqrt{s} = 1$ TeV with an integrated luminosity of 1 ab⁻¹. The three sigma contours for χ^2 analysis in $m_{\text{DM}} - \Lambda_{\text{eff}}$ plane are drawn in figures 8a and 8b corresponding to the lepto-philic and B-philic respectively for case (i) and similarly, contours corresponding to case (ii) are shown in figures 8c and 8d respectively.

We hope this study will be useful in studying the physics potential of the ILC in context to dark matter searches.

Acknowledgments

HB and SD thank Mihoko Nojiri for discussions and suggestions throughout the work. HB acknowledges the CSIR-JRF fellowship. HB and SD acknowledge the partial financial support from the CSIR grant No. 03(1340)/15/EMR-II. SD thanks the Theory Division, KEK, for an excellent hospitality where this problem was conceived.

Appendix

A Thermal averaged annihilation cross-sections

The fermionic, scalar and vector DM pair annihilation cross sections to SM l^+l^- pairs of mass m_l induced by the *lepto-philic* twist-2 operators are given by

$$\begin{aligned} \sigma_{T_1}^{\text{ann}} (\chi\bar{\chi} \rightarrow l^+l^-) = & \\ \frac{\pi\alpha_{T_1}^2}{s} \left(\frac{m_\chi^2}{\Lambda_{\text{eff}}^6} \right) \sqrt{\frac{s-4m_l^2}{s-4m_\chi^2}} & \left[16m_l^2 m_\chi^2 + 32m_\chi^4 + \left(9m_l^2 m_\chi^2 - \frac{11}{3}m_l^4 + \frac{14}{3}m_\chi^4 \right) |\vec{v}|^2 \right] \end{aligned} \quad (\text{A.1})$$

$$\sigma_{T_2}^{\text{ann}} (\chi\bar{\chi} \rightarrow l^+l^-) = \frac{\pi\alpha_{T_2}^2}{s} \left(\frac{m_\chi^2}{\Lambda_{\text{eff}}^6} \right) \sqrt{\frac{s-4m_l^2}{s-4m_\chi^2}} m_l^2 (m_\chi^2 - m_l^2) |\vec{v}|^2 \quad (\text{A.2})$$

$$\begin{aligned} \sigma_S^{\text{ann}} (\phi^0\phi^0 \rightarrow l^+l^-) = & \\ \frac{\pi\alpha_{\phi^0}^2}{s} \left(\frac{m_{\phi^0}^2}{\Lambda_{\text{eff}}^4} \right) \sqrt{\frac{s-4m_l^2}{s-4m_{\phi^0}^2}} & \left[2m_l^2 - \frac{2m_l^4}{m_{\phi^0}^2} + \left(\frac{4}{3}\frac{m_l^4}{m_{\phi^0}^2} + \frac{11}{6}m_l^2 + \frac{16}{3}m_{\phi^0}^2 \right) |\vec{v}|^2 \right] \end{aligned} \quad (\text{A.3})$$

$$\begin{aligned} \sigma_V^{\text{ann}} (V^0V^0 \rightarrow l^+l^-) = & \\ \frac{\pi\alpha_{V^0}^2}{s} \left(\frac{m_{V^0}^2}{\Lambda_{\text{eff}}^4} \right) \sqrt{\frac{s-4m_l^2}{s-4m_{V^0}^2}} & \left[\frac{2}{3}m_l^2 - \frac{2}{3}\frac{m_l^4}{m_{V^0}^2} + \left(\frac{2}{9}\frac{m_l^4}{m_{V^0}^2} + \frac{5}{6}m_l^2 + \frac{16}{9}m_{V^0}^2 \right) |\vec{v}|^2 \right] \end{aligned} \quad (\text{A.4})$$

The fermionic, scalar and vector DM pair annihilation cross sections to photon pairs induced by the $U(1)_Y$ Boson B -philic twist-2 operators are given by

$$\sigma_{T_1}^{\text{ann}}(\chi\bar{\chi} \rightarrow \gamma\gamma) = \frac{8\pi\alpha_{T_1}^2}{3s} \cos^2\theta_W \frac{m_\chi^6}{\Lambda_{\text{eff}}^6} \sqrt{\frac{s}{s-4m_\chi^2}} |\vec{v}|^2 \quad (\text{A.5})$$

$$\sigma_{T_2}^{\text{ann}}(\chi\bar{\chi} \rightarrow \gamma\gamma) = \frac{\pi\alpha_{T_2}^2}{s} \cos^2\theta_W \frac{m_\chi^6}{\Lambda_{\text{eff}}^6} \sqrt{\frac{s}{s-4m_\chi^2}} |\vec{v}|^2 \quad (\text{A.6})$$

$$\sigma_S^{\text{ann}}(\phi^0\phi^0 \rightarrow \gamma\gamma) = \frac{2\pi\alpha_{\phi^0}^2}{s} \cos^2\theta_W \frac{m_{\phi^0}^4}{\Lambda_{\text{eff}}^4} \sqrt{\frac{s}{s-4m_{\phi^0}^2}} \left[1 + \frac{2}{3} |\vec{v}|^2\right] \quad (\text{A.7})$$

$$\sigma_V^{\text{ann}}(V^0V^0 \rightarrow \gamma\gamma) = \frac{2\pi\alpha_{V^0}^2}{3s} \cos^2\theta_W \frac{m_{V^0}^4}{\Lambda_{\text{eff}}^4} \sqrt{\frac{s}{s-4m_{V^0}^2}} \left[1 + |\vec{v}|^2\right] \quad (\text{A.8})$$

where $\cos\theta_W$ is the Weinberg mixing angle.

The DM relic density is given in terms of thermally averaged DM annihilation cross sections $\langle\sigma_{\text{ann}}|\vec{v}|\rangle$ in equation (3.2). To compute the same we express the relative velocity of DM pair in the laboratory frame $|\vec{v}|$ in terms of c.m. energy \sqrt{s} as

$$|\vec{v}| = \frac{\sqrt{s(s-4m_{\text{DM}}^2)}}{s-2m_{\text{DM}}^2}. \quad (\text{A.9})$$

Since $v \ll c$, for non-relativistic DM we expand $s = 4m_{\text{DM}}^2 + m_{\text{DM}}^2 |\vec{v}|^2 + \frac{3}{4} m_{\text{DM}}^2 |\vec{v}|^4 + \mathcal{O}(|\vec{v}|^6)$ and compute the thermally averaged annihilation cross sections for lepto-philic and $U(1)_Y$ gauge Boson-philic DM respectively.

Thermal averaged annihilation cross-sections corresponding to the cross-sections given in equations (A.1) - (A.4) for the lepto-philic operators are given respectively as

$$\langle\sigma_{T_1}^{\text{ann}}|\vec{v}|\rangle(\chi\bar{\chi} \rightarrow l^+l^-) = \pi\alpha_{T_1}^2 \left(\frac{m_\chi^4}{\Lambda_{\text{eff}}^6}\right) \sqrt{1 - \frac{m_l^2}{m_\chi^2}} \left[1 + \frac{m_l^2}{2m_\chi^2} - \frac{34}{96} \frac{6}{x_F}\right] \quad (\text{A.10})$$

$$\langle\sigma_{T_2}^{\text{ann}}|\vec{v}|\rangle(\chi\bar{\chi} \rightarrow l^+l^-) = \frac{\pi\alpha_{T_2}^2}{2} \left(\frac{m_l^2 m_\chi^2}{\Lambda_{\text{eff}}^6}\right) \left[1 - \frac{m_l^2}{m_\chi^2}\right]^{\frac{3}{2}} \frac{6}{x_F} \quad (\text{A.11})$$

$$\begin{aligned} \langle\sigma_S^{\text{ann}}|\vec{v}|\rangle(\phi^0\phi^0 \rightarrow l^+l^-) &= \pi\alpha_{\phi^0}^2 \left(\frac{m_{\phi^0}^2}{\Lambda_{\text{eff}}^4}\right) \sqrt{1 - \frac{m_l^2}{m_{\phi^0}^2}} \\ &\times \left[\frac{m_l^2}{m_{\phi^0}^2} - \frac{m_l^4}{m_{\phi^0}^4} + \left(\frac{8}{3} + \frac{11}{12} \frac{m_l^2}{m_{\phi^0}^2} + \frac{2}{3} \frac{m_l^4}{m_{\phi^0}^4}\right) \frac{6}{x_F}\right] \end{aligned} \quad (\text{A.12})$$

$$\begin{aligned} \langle\sigma_V^{\text{ann}}|\vec{v}|\rangle(V^0V^0 \rightarrow l^+l^-) &= \frac{8\pi\alpha_{V^0}^2}{9} \left(\frac{m_{V^0}^2}{\Lambda_{\text{eff}}^4}\right) \sqrt{1 - \frac{m_l^2}{m_{V^0}^2}} \\ &\times \left[\frac{3}{8} \frac{m_l^2}{m_{V^0}^2} - \frac{3}{8} \frac{m_l^4}{m_{V^0}^4} + \left(1 + \frac{15}{32} \frac{m_l^2}{m_{V^0}^2} + \frac{1}{8} \frac{m_l^4}{m_{V^0}^4}\right) \frac{6}{x_F}\right] \end{aligned} \quad (\text{A.13})$$

Similarly, the annihilation cross-sections given in equations (A.5)-(A.8) for the $U(1)_Y$ gauge Boson B -philic operators are thermalized to give the following thermal averaged annihilation

cross-sections:

$$\langle \sigma_{T_1}^{\text{ann}} | \vec{v} \rangle (\chi \bar{\chi} \rightarrow \gamma \gamma) = \frac{4\pi\alpha_{T_1}^2}{3} \cos^2 \theta_W \left(\frac{m_\chi^4}{\Lambda_{\text{eff}}^6} \right) \frac{6}{x_F} \quad (\text{A.14})$$

$$\langle \sigma_{T_2}^{\text{ann}} | \vec{v} \rangle (\chi \bar{\chi} \rightarrow \gamma \gamma) = \frac{4\pi\alpha_{T_2}^2}{2} \cos^2 \theta_W \left(\frac{m_\chi^4}{\Lambda_{\text{eff}}^6} \right) \frac{6}{x_F} \quad (\text{A.15})$$

$$\langle \sigma_S^{\text{ann}} | \vec{v} \rangle (\phi^0 \phi^0 \rightarrow \gamma \gamma) = \pi\alpha_{\phi^0}^2 \cos^2 \theta_W \left(\frac{m_{\phi^0}^2}{\Lambda_{\text{eff}}^4} \right) \left[1 + \frac{1}{6} \frac{6}{x_F} \right] \quad (\text{A.16})$$

$$\langle \sigma_V^{\text{ann}} | \vec{v} \rangle (V^0 V^0 \rightarrow \gamma \gamma) = \frac{\pi\alpha_{V^0}^2}{3} \cos^2 \theta_W \left(\frac{m_{V^0}^2}{\Lambda_{\text{eff}}^4} \right) \left[1 + \frac{1}{2} \frac{6}{x_F} \right] \quad (\text{A.17})$$

References

- [1] G. Bertone, D. Hooper and J. Silk, Phys. Rept. **405**, 279 (2005) doi:10.1016/j.physrep.2004.08.031 [hep-ph/0404175].
- [2] V. C. Rubin and W. K. Ford, Jr., *Astroph. J.* **159** (1970) 379.
- [3] L. A. Moustakas and R. B. Metcalf, Mon. Not. Roy. Astron. Soc. **339**, 607 (2003) doi:10.1046/j.1365-8711.2003.06055.x [astro-ph/0206176].
- [4] M. Milgrom, *Astrophys. J.* **270**, 365 (1983). doi:10.1086/161130
- [5] D. Clowe, M. Bradac, A. H. Gonzalez, M. Markevitch, S. W. Randall, C. Jones and D. Zaritsky, *Astrophys. J.* **648**, L109 (2006) doi:10.1086/508162 [astro-ph/0608407].
- [6] E. van Uitert *et al* *Astron. Astroph.* **545** A71(2012) [arXiv:1206.4304].
- [7] E. Komatsu *et al.* [WMAP Science Team], *PTEP* **2014**, 06B102 (2014) doi:10.1093/ptep/ptu083 [arXiv:1404.5415 [astro-ph.CO]].
- [8] P. A. R. Ade *et al.* [Planck Collaboration], *Astron. Astrophys.* **594**, A13 (2016) doi:10.1051/0004-6361/201525830 [arXiv:1502.01589 [astro-ph.CO]].
- [9] T. M. Hong, arXiv:1709.02304 [hep-ex].
- [10] F. Kahlhoefer, *Int. J. Mod. Phys. A* **32**, no. 13, 1730006 (2017) doi:10.1142/S0217751X1730006X [arXiv:1702.02430 [hep-ph]].
- [11] V. A Mitsou, **2015** *J. Phys.: Conf. Ser.* 651 012023 doi:10.1088/1742-6596/651/1/012023.
- [12] H. Dreiner, M. Huck, M. Krüger, D. Schmeier and J. Tattersall, *Phys. Rev. D* **87**, no. 7, 075015 (2013) doi:10.1103/PhysRevD.87.075015 [arXiv:1211.2254 [hep-ph]].
- [13] M. Battaglia and M. E. Peskin, *eConf C* **050318**, 0709 (2005) [hep-ph/0509135].
- [14] S. Dutta, D. Sachdeva and B. Rawat, *Eur. Phys. J. C* **77**, no. 9, 639 (2017) doi:10.1140/epjc/s10052-017-5188-8 [arXiv:1704.03994 [hep-ph]].
- [15] R. Bernabei *et al.*, *Eur. Phys. J. C* **73**, 2648 (2013) doi:10.1140/epjc/s10052-013-2648-7 [arXiv:1308.5109 [astro-ph.GA]].
- [16] R. Bernabei *et al.*, arXiv:1805.10486 [hep-ex].
- [17] C. E. Aalseth *et al.* [CoGeNT Collaboration], *Phys. Rev. D* **88**, 012002 (2013) doi:10.1103/PhysRevD.88.012002 [arXiv:1208.5737 [astro-ph.CO]].

- [18] G. Angloher *et al.* [CRESST Collaboration], *Eur. Phys. J. C* **77**, no. 5, 299 (2017) doi:10.1140/epjc/s10052-017-4878-6 [arXiv:1612.07662 [hep-ex]].
- [19] R. Agnese *et al.* [CDMS Collaboration], *Phys. Rev. Lett.* **111** (2013) no.25, 251301 doi:10.1103/PhysRevLett.111.251301 [arXiv:1304.4279 [hep-ex]].
- [20] E. Aprile *et al.* [XENON100 Collaboration], *Phys. Rev. D* **94** (2016) no.12, 122001 doi:10.1103/PhysRevD.94.122001 [arXiv:1609.06154 [astro-ph.CO]].
- [21] E. Aprile *et al.* [XENON Collaboration], *Eur. Phys. J. C* **77** (2017) no.12, 881 doi:10.1140/epjc/s10052-017-5326-3 [arXiv:1708.07051 [astro-ph.IM]].
- [22] D. S. Akerib *et al.* [LUX Collaboration], *Phys. Rev. Lett.* **118** (2017) no.2, 021303 doi:10.1103/PhysRevLett.118.021303 [arXiv:1608.07648 [astro-ph.CO]].
- [23] X. Cui *et al.* [PandaX-II Collaboration], *Phys. Rev. Lett.* **119** (2017) no.18, 181302 doi:10.1103/PhysRevLett.119.181302 [arXiv:1708.06917 [astro-ph.CO]].
- [24] M. Ackermann *et al.* [Fermi-LAT Collaboration], *Phys. Rev. Lett.* **115** (2015) no.23, 231301 doi:10.1103/PhysRevLett.115.231301 [arXiv:1503.02641 [astro-ph.HE]].
- [25] M. Ajello *et al.* [Fermi-LAT Collaboration], *Astrophys. J.* **819** (2016) no.1, 44 doi:10.3847/0004-637X/819/1/44 [arXiv:1511.02938 [astro-ph.HE]].
- [26] A. Albert *et al.* [Fermi-LAT and DES Collaborations], *Astrophys. J.* **834** (2017) no.2, 110 doi:10.3847/1538-4357/834/2/110 [arXiv:1611.03184 [astro-ph.HE]].
- [27] A. Abramowski *et al.* [H.E.S.S. Collaboration], *Phys. Rev. Lett.* **110** (2013) 041301 doi:10.1103/PhysRevLett.110.041301 [arXiv:1301.1173 [astro-ph.HE]].
- [28] M. Aguilar *et al.* [AMS Collaboration], *Phys. Rev. Lett.* **113** (2014) 121102. doi:10.1103/PhysRevLett.113.121102
- [29] M. Aguilar *et al.* [AMS Collaboration], *Phys. Rev. Lett.* **117** (2016) no.9, 091103. doi:10.1103/PhysRevLett.117.091103
- [30] O. Adriani *et al.* [PAMELA Collaboration], *Phys. Rev. Lett.* **111**, 081102 (2013) doi:10.1103/PhysRevLett.111.081102 [arXiv:1308.0133 [astro-ph.HE]].
- [31] O. Adriani *et al.* [PAMELA Collaboration], *Nature* **458**, 607 (2009) doi:10.1038/nature07942 [arXiv:0810.4995 [astro-ph]].
- [32] A. D. Panov *et al.*, *Bull. Russ. Acad. Sci. Phys.* **71** (2007) 494 doi:10.3103/S1062873807040168 [astro-ph/0612377].
- [33] K. Yoshida, et al., 42 (Nov., 2008) 1670a–1675, doi:10.1016/j.asr.2007.04.043.
- [34] G. Ambrosi *et al.* [DAMPE Collaboration], *Nature* **552** (2017) 63 doi:10.1038/nature24475 [arXiv:1711.10981 [astro-ph.HE]].
- [35] T. Appelquist, H. C. Cheng and B. A. Dobrescu, *Phys. Rev. D* **64** (2001) 035002 doi:10.1103/PhysRevD.64.035002 [hep-ph/0012100].
- [36] J. Wess and B. Zumino, *Nucl. Phys. B* **70** (1974) 39. doi:10.1016/0550-3213(74)90355-1
- [37] H. P. Nilles, *Phys. Rept.* **110** (1984) 1. doi:10.1016/0370-1573(84)90008-5
- [38] M. Drees, R. Godbole, P. Roy, "Theory and phenomenology of sparticles: an account of four-dimensional N=1 supersymmetry in high energy physics" (2004).
- [39] N. Arkani-Hamed, A. G. Cohen, H. Georgy, *Phys. Lett. B* **513**,232-C240 (2001).

- [40] H. C. Cheng, I. Low, JHEP **0309**, 051 (2003), doi: 10.1088/1126-6708/2003/09/051, [arXiv:hep-ph/0308199].
- [41] S. Dutta, A. Goyal and M. P. Singh, arXiv:1809.07877 [hep-ph].
- [42] J. M. Zheng, Z. H. Yu, J. W. Shao, X. J. Bi, Z. Li and H. H. Zhang, Nucl. Phys. B **854** (2012) 350 doi:10.1016/j.nuclphysb.2011.09.009 [arXiv:1012.2022 [hep-ph]].
- [43] A. Freitas and S. Westhoff, JHEP **1410** (2014) 116 doi:10.1007/JHEP10(2014)116 [arXiv:1408.1959 [hep-ph]].
- [44] K. G. Savvidy and J. D. Vergados, Phys. Rev. D **87** (2013) no.7, 075013 doi:10.1103/PhysRevD.87.075013 [arXiv:1211.3214 [hep-ph]].
- [45] C. F. Chang, X. G. He and J. Tandean, Phys. Rev. D **96** (2017) no.7, 075026 doi:10.1103/PhysRevD.96.075026 [arXiv:1704.01904 [hep-ph]].
- [46] S. Dutta, A. Goyal and L. K. Saini, JHEP **1802** (2018) 023 doi:10.1007/JHEP02(2018)023 [arXiv:1709.00720 [hep-ph]].
- [47] B. Bhattacharjee, D. Choudhury, K. Harigaya, S. Matsumoto and M. M. Nojiri, JHEP **1304** (2013) 031 doi:10.1007/JHEP04(2013)031 [arXiv:1212.5013 [hep-ph]].
- [48] R. C. Cotta, J. L. Hewett, M. P. Le and T. G. Rizzo, Phys. Rev. D **88** (2013) 116009 doi:10.1103/PhysRevD.88.116009 [arXiv:1210.0525 [hep-ph]].
- [49] J. Y. Chen, E. W. Kolb and L. T. Wang, Phys. Dark Univ. **2** (2013) 200 doi:10.1016/j.dark.2013.11.002 [arXiv:1305.0021 [hep-ph]].
- [50] A. Crivellin, U. Haisch and A. Hibbs, Phys. Rev. D **91** (2015) 074028 doi:10.1103/PhysRevD.91.074028 [arXiv:1501.00907 [hep-ph]].
- [51] N. Chen, J. Wang and X. P. Wang, arXiv:1501.04486 [hep-ph].
- [52] P. J. Fox, R. Harnik, J. Kopp and Y. Tsai, Phys. Rev. D **85** (2012) 056011 doi:10.1103/PhysRevD.85.056011 [arXiv:1109.4398 [hep-ph]].
- [53] Y. J. Chae and M. Perelstein, “*Dark Matter Search at a Linear Collider: Effective Operator Approach*”, JHEP **1305** (2013) 138 [arXiv:1211.4008 [hep-ph]].
- [54] N. F. Bell, J. B. Dent, A. J. Galea, T. D. Jacques, L. M. Krauss and T. J. Weiler, Phys. Rev. D **86** (2012) 096011 doi:10.1103/PhysRevD.86.096011 [arXiv:1209.0231 [hep-ph]].
- [55] M. Drees and M. Nojiri, Phys. Rev. D **48** (1993) 3483 doi:10.1103/PhysRevD.48.3483 [hep-ph/9307208].
- [56] J. Hisano, K. Ishiwata and N. Nagata, Phys. Rev. D **82** (2010) 115007 doi:10.1103/PhysRevD.82.115007 [arXiv:1007.2601 [hep-ph]].
- [57] J. Hisano, K. Ishiwata, N. Nagata and M. Yamanaka, Prog. Theor. Phys. **126** (2011) 435 doi:10.1143/PTP.126.435 [arXiv:1012.5455 [hep-ph]].
- [58] J. Hisano, K. Ishiwata, N. Nagata and T. Takesako, JHEP **1107** (2011) 005 doi:10.1007/JHEP07(2011)005 [arXiv:1104.0228 [hep-ph]].
- [59] J. Hisano, K. Ishiwata and N. Nagata, Phys. Lett. B **706** (2011) 208 doi:10.1016/j.physletb.2011.11.017 [arXiv:1110.3719 [hep-ph]].
- [60] J. Hisano, K. Ishiwata and N. Nagata, Phys. Rev. D **87** (2013) 035020 doi:10.1103/PhysRevD.87.035020 [arXiv:1210.5985 [hep-ph]].

- [61] J. Hisano, R. Nagai and N. Nagata, JHEP **1505** (2015) 037 doi:10.1007/JHEP05(2015)037 [arXiv:1502.02244 [hep-ph]].
- [62] J. Hisano, K. Ishiwata and N. Nagata, JHEP **1506** (2015) 097 doi:10.1007/JHEP06(2015)097 [arXiv:1504.00915 [hep-ph]].
- [63] F. Ambrogio, C. Arina, M. Backovic, J. Heisig, F. Maltoni, L. Mantani, O. Mattelaer and G. Mohlabeng, arXiv:1804.00044 [hep-ph].
- [64] J. Alwall *et al.*, JHEP **1407** (2014) 079 doi:10.1007/JHEP07(2014)079 [arXiv:1405.0301 [hep-ph]].
- [65] A. Alloul, N. D. Christensen, C. Degrande, C. Duhr and B. Fuks, Comput. Phys. Commun. **185** (2014) 2250 doi:10.1016/j.cpc.2014.04.012 [arXiv:1310.1921 [hep-ph]].
- [66] J. Kopp, V. Niro, T. Schwetz and J. Zupan, “*DAMA/LIBRA and leptonically interacting Dark Matter*”, Phys. Rev. D **80**, 083502 (2009) [arXiv:0907.3159 [hep-ph]].
- [67] E. Aprile *et al.* [XENON100 Collaboration], “*Exclusion of Leptophilic Dark Matter Models using XENON100 Electronic Recoil Data*”, Science **349**, no. 6250, 851 (2015) doi:10.1126/science.aab2069 [arXiv:1507.07747 [astro-ph.CO]].
- [68] S. Schael *et al.* [ALEPH and DELPHI and L3 and OPAL and LEP Electroweak Collaborations], Phys. Rept. **532**, 119 (2013) doi:10.1016/j.physrep.2013.07.004 [arXiv:1302.3415 [hep-ex]].
- [69] E. Conte and B. Fuks, Int. J. Mod. Phys. A **33**, no. 28, 1830027 (2018) doi:10.1142/S0217751X18300272 [arXiv:1808.00480 [hep-ph]].
- [70] E. Conte, B. Fuks and G. Serret, Comput. Phys. Commun. **184**, 222 (2013) doi:10.1016/j.cpc.2012.09.009 [arXiv:1206.1599 [hep-ph]].
- [71] T. Behnke *et al.*, arXiv:1306.6329 [physics.ins-det].
- [72] T. Behnke *et al.*, “The International Linear Collider Technical Design Report - Volume 1: Executive Summary,” arXiv:1306.6327 [physics.acc-ph].